Hydrodynamic Origin of Diffusion in Nanopores

Suresh K. Bhatia* and David Nicholson†

Department of Chemical Engineering, The University of Queensland, Brisbane QLD 4072, Australia

(Received 18 August 2002; published 9 January 2003)

We study the transport of a subcritical Lennard-Jones fluid in a cylindrical nanopore, using a combination of equilibrium and nonequilibrium as well as dual control volume grand canonical molecular dynamics methods. We show that all three techniques yield the same value of the transport coefficient for diffusely reflecting pore walls, even in the presence of viscous transport. We also demonstrate that the classical Knudsen mechanism is not manifested, and that a combination of viscous flow and momentum exchange at the pore wall governs the transport over a wide range of densities.

DOI: 10.1103/PhysRevLett.90.016105 PACS numbers: 68.43.Jk

Intense worldwide activity in applications of newly developed templated porous materials, carbon nanotubes, and a variety of related materials [1,2] has led to renewed interest in the long-standing problem of modeling transport in nanopores. Generally, this is represented in a diffusional framework with a concentration dependent diffusivity [3–5]; however, there is much controversy regarding the underlying mechanisms. It has for some time been considered that transport in confined spaces, such as in nanopores, comprises a purely diffusive component, as well as a hydrodynamic or viscous component [6,7]. Various simulation techniques such as equilibrium molecular dynamics (EMD), nonequilibrium molecular dynamics (NEMD), and dual control volume grand canonical molecular dynamics (DCV-GCMD) have been designed [8,9] and applied to probe the different mechanisms, and to verify proposed models. Nevertheless, an unequivocal description of the transport has not emerged, partly because the proposed models [6,7,10,11] have arbitrary fitting parameters. The diffusive component is often considered dominant [11] and arbitrarily treated as activated surface flow [11], Knudsen diffusion [4,6,7,11], or slip flow [12,13], particularly at low coverage, and in pores of near-molecular width, where the hydrodynamic approaches [10] predict a vanishing transport coefficient contrary to experiment or simulations [3–5].

It has been argued [14] that the transport coefficient obtained by DCV-GCMD simulation, in which the flux in a finite capillary under the action of a chemical potential gradient is measured, represents the combined effects of diffusive and viscous flow, while NEMD, in which the steady state flux in an infinite capillary under the action of a constant force is measured, should yield only the viscous component. On the other hand, it has also been surmised [5] that EMD should yield only the diffusive component since bulk flow is absent in this method. More recently, it has been found [15] that all three techniques yield the same transport coefficient in micropores, where viscous flow is considered negligible. This therefore still leaves open the question regarding the differences between the methods in larger pores where viscous transport is significant. Here we show that for single component flow in mesopores with diffusely reflecting walls the different simulation techniques yield equivalent results, and that in real porous materials dispersive forces cause momentum transfer at the wall to dominate over strictly diffusive mechanisms. Thus, the transport coefficient even at low densities can be explained by hydrodynamic mechanisms alone.

The simulations conducted model the flow of Lennard-Jones (LJ) methane at 150 and 177 K in a cylindrical silica pore of radius 1.919 nm, having infinitely thick pore walls comprising spherical LJ sites. For methane, we use the established LJ parameter values $e_f/k_B = 148.2$ K, $\sigma_f = 0.381$ nm. For the solid LJ parameters, we use $\varepsilon_s/k_B = 290$ K, $\sigma_s = 0.29$ nm, obtained by fitting argon isotherms at 87 K in MCM-41 of various pore diameters [16], using grand canonical Monte Carlo (GCMC) simulation. The Lorentz-Berthelot rules are used to estimate solid-fluid LJ interaction parameters. A cutoff separation of 1.5 nm is used in computing fluid-fluid potentials.

In the molecular dynamics calculations, the trajectories of methane molecules in the pore are followed using the equation of motion,

$$\ddot{\boldsymbol{r}}_i = -\frac{1}{m}\sum_{j\neq i}\nabla_i\Phi_{ij} + \boldsymbol{\Gamma} - \lambda(t)\dot{\boldsymbol{r}}_i, \tag{1}$$

starting from an arbitrary initial configuration generated using GCMC simulation at a chosen chemical potential. Here Φ_{ij} is the potential energy due to the i-j interaction, $\boldsymbol{\Gamma}$ is a constant acceleration externally applied to every particle, and $\lambda(t)$ a thermostat factor [17]. A fifth order Gear predictor-corrector method with a time step of 2 fs is used to solve the equations of motion. Particles closer to the wall than the minimum of the fluid-solid potential are diffusely scattered in the osculating plane at the pore wall, and their tangential as well as axial velocity randomized, when while moving towards the wall the radial component of the velocity is reversed.

For the EMD simulations, no external acceleration is applied on the particles (i.e., $\boldsymbol{\Gamma} = 0$) and a collective transport coefficient obtained from autocorrelation of

the fluctuating axial streaming velocity via a Green-Kubo relation [5]

$$D_{to} = N \lim_{\tau\to\infty} \int_o^\tau \langle u_z(0) u_z(t)\rangle dt, \qquad (2)$$

where $u_z(t) = \sum dz_i/dt$. From a transport point of view, it is this collective coefficient that is relevant, as opposed to the more commonly studied self-diffusivity that applies to tracer diffusion. For the NEMD simulations, a constant axial acceleration Γ_z in the range of 0.01–0.1 nm/ps^2 is applied to the particles, and a transport coefficient computed from the measured flux as $D_{to} = k_B T \boldsymbol{j}/\hat{\boldsymbol{\rho}} m \Gamma$, where $\boldsymbol{j}$ is the axial number flux and $\hat{\boldsymbol{\rho}}$ is the methane density in the pore. For the DCV-GCMD simulations, a three zone method is used [5,9], with $\boldsymbol{\Gamma} = 0$, but with the two end zones maintained at different chemical potentials. An effective Fickian transport coefficient is then computed from the measured flux through $D_{t,\mathrm{eff}} = -\boldsymbol{j}\ell/\Delta\rho$, where ℓ is the length of the central gradient zone and $\Delta\rho$ the applied density difference.

To our surprise, the different transport coefficient obtained at various densities from the three MD techniques were essentially identical. Figure 1 depicts the transport coefficients from EMD and NEMD at the two temperatures, showing essentially no difference. Clear evidence of an asymptotic nonzero transport coefficient at low densities is also seen, with only weak density dependence in this region. The inset depicts the comparison of a purely no-slip viscous theory, to be discussed below, with the NEMD results at 150 K, showing good correspondence at moderate and high densities, and failure at low densities where the latter predicts a vanishing transport coefficient. Despite the latter deviation, the general trends are similar, in particular, a nearly constant transport coefficient below a density of about 4 nm^{-3} (after an initial increase from a value of zero for the theory). This roughly corresponds to the monolayer region, based on a molecular area of about 0.195 nm^2 estimated from its liquid density of 13.5 nm^{-3} at 150 K. The good agreement at high density and similarity in trend does suggest the role of viscous effects in the transport, though an additional mechanism is also signified by the quantitative disagreement at low densities.

The above correspondence contradicts recent assertions [5,14] that EMD measures only the diffusive component and NEMD the viscous component of the transport coefficient. Our results clearly indicate that the EMD transport coefficient does include the viscous part, despite the absence of imposed bulk flow. This implies that the relaxation time of the viscous stresses is smaller than the time scale of the fluctuations induced by diffuse reflection at the wall, and the resulting fluctuating streaming velocity profiles are at instantaneous equilibrium. As evidence of cross-sectional equilibrium, comparison of density distributions obtained from GCMC simulation with those from EMD and NEMD simulation showed all three to be essentially identical over the whole

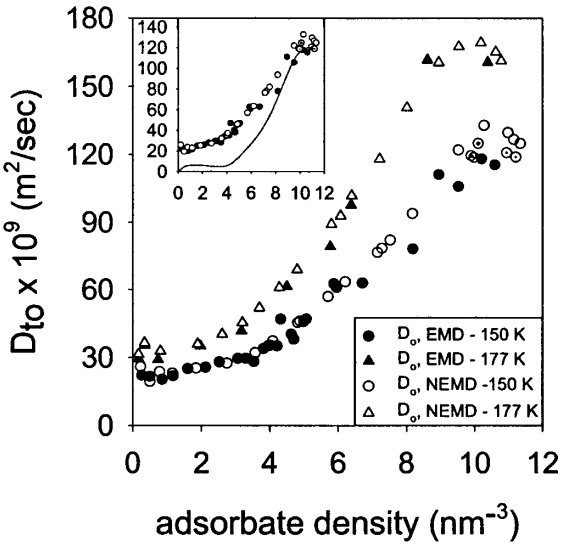

FIG. 1. Variation of transport coefficient with density. The inset depicts the comparison of a purely no-slip viscous theory with the NEMD results at 150 K. Open circles with cross hair represent data obtained with acceleration of 0.07 nm/ps^2, and open circles with dots with acceleration of 0.1 nm/ps^2. All other data obtained with acceleration of 0.04 nm/ps^2, or less.

range of densities. The inset of Fig. 2 shows one such correspondence, obtained for a pore density of 5.95 nm^{-3}.

A large number of DCV-GCMC runs were also conducted at 150 K, for various pair of density values in the two end sections, and the effective Fickian transport coefficient, $D_{t,\mathrm{eff}}$, obtained. A similar coefficient is also estimated from the EMD and NEMD values of D_{to}, which correspond to a chemical potential gradient driving force, following

$$D_{t,\mathrm{eff}} = -\frac{\boldsymbol{j}\ell}{\Delta\rho} = \frac{1}{\Delta\rho}\int_{\rho_1}^{\rho_2} D_{to}(\rho)\left(\frac{\partial \ln f}{\partial \ln \rho}\right)_T d\rho, \qquad (3)$$

which matches that from DCV-GCMD, as seen in Fig. 2, over the wide range of densities covered. Here f is the bulk fugacity of methane in equilibrium with adsorbed density ρ, and the associated derivative is estimated from isotherms obtained by GCMC simulation. Thus, it is clear that neither NEMD nor DCV-GCMD probes any new mechanism beyond that captured by EMD simulations.

While confirming that all three simulation methods effectively measure the same transport coefficient for diffusely reflecting walls, the results beg further analysis to uncover the underlying mechanisms. Our theoretical calculations indicated viscous flow to be dominant at high densities, as depicted by the agreement of the theory in the inset of Fig. 1. To obtain the theoretical curve, we solved the Navier Stokes equation,

$$\frac{1}{r}\frac{d}{dr}\left[r\eta(r)\frac{du_z}{dr}\right] = \frac{\partial P}{\partial z} = \rho(r)\frac{d\mu}{dz}, \qquad (4)$$

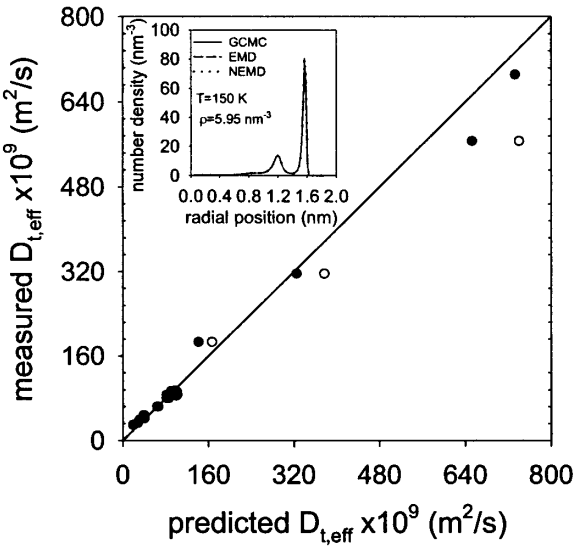

FIG. 2. Comparison of measured transport coefficients, obtained using DCV-GCMD, with those predicted based on coefficients obtained using EMD (filled circles) and NEMD (open circles). The inset shows that equilibrium density profiles are attained in EMD and NEMD.

assuming cross-sectional equilibrium with a no-slip boundary condition, to obtain the transport coefficient,

$$D_{to}(\hat{\rho}) = \frac{2k_BT}{R_s^2\hat{\rho}} \int_0^{r_o} \frac{dr}{r\eta(r)} \left[\int_0^r r'\rho(r')dr' \right]^2. \quad (5)$$

Here R_s represents the pore radius measured from the center of the surface atoms, and $\hat{\rho} = 2\int_0^{R_s} r\rho(r)dr/R_s^2$ is the mean pore density. The radial density profile $\rho(r)$ is obtained from simulations, while the local viscosity is evaluated using the method of Chung *et al.* [18], at a density locally averaged over a sphere of radius $\sigma_f/2$ [19]. The radius r_o in Eq. (5) represents the position of the minimum of the fluid-solid potential, which is essentially the location of the reflection boundary.

While both theory and simulation yield agreement at high densities, as seen in Fig. 1, the measured nonvanishing transport coefficient at low densities does suggest a significant degree of slip not considered in the theory. To capture this, we consider the surface boundary condition,

$$k\rho_o u_o = -\eta \frac{du_z}{dr} \quad \text{at } r = r_o, \quad (6)$$

where ρ_o is the local density at the potential minimum, u_o is the slip velocity, and k a friction coefficient. Solution of Eqs. (4) and (6) yields the transport coefficient,

$$D_{to}(\hat{\rho}) = \frac{2k_BT}{R_s^2\hat{\rho}} \left[\frac{1}{k\rho_o r_o} \left(\int_0^{r_o} r\rho(r)dr \right)^2 + \int_0^{r_o} \frac{dr}{r\eta(r)} \left(\int_0^r r'\rho(r')dr' \right)^2 \right], \quad (7)$$

in place of Eq. (5), which predicts an asymptotic nonvanishing transport coefficient in the low-density region.

The variation of the friction coefficient k with local density ρ_o at the surface of friction (the location of the potential minimum) can be obtained by substituting the values of D_{to} and density profile $\rho(r)$ obtained from NEMD simulation at density $\hat{\rho}$ into Eq. (7). Figure 3 depicts the results, obtained using the NEMD transport coefficients with an acceleration of 0.04 nm/ps^2, showing a relatively constant value of the friction coefficient k of about 1.2–1.6 N · sec·mole^{-1} at 150 K and 1.3–1.7 N · sec·mole^{-1} at 177 K, for local density ρ_o below a critical value (about 85 nm^{-3} at 150 K, and 75 nm^{-3} at 177 K). Subsequently, it increases steeply to very large values, approaching the no-slip condition at high densities.

The constancy of the friction coefficient is a strong indicator of the importance of slip flow at the pore wall in nanopores. Further, calculations showed that the above values of the friction constant are closely consistent with momentum transfer arguments [7,20]. For this, we consider the frictional force as arising from the momentum loss on diffuse reflection at the wall leading to

$$k\rho_o u_o = mu_o Z, \quad (8)$$

where Z ($= \rho_o\bar{v}/4$) is the collision frequency under conditions of local equilibrium. Substitution of the kinetic theory result $\bar{v} = (8k_BT/\pi m)^{1/2}$ yields $k = \sqrt{mk_BT/2\pi}$, providing the estimates $k = 1.78$ N · sec·mole^{-1} at 150 K and 1.94 N · sec·mole^{-1} at 177 K, in remarkably good agreement with the values obtained from the simulation results. Further support is obtained from comparison of the predicted streaming velocity profile from solution of Eq. (4) with that obtained from NEMD simulation. The inset of Fig. 3 depicts one such comparison, obtained for an adsorbed density of 5.95 nm^{-3} at 150 K and imposed

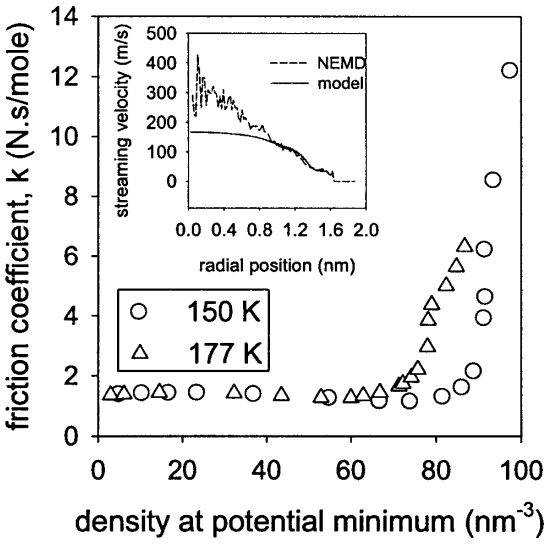

FIG. 3. Variation of friction factor with density at potential minimum, obtained at temperatures of 150 and 177 K. The inset depicts predicted and measured streaming velocity profile at adsorbed density of 5.95 nm^{-3} and temperature of 150 K.

acceleration of 0.07 nm/ps^2. Excellent agreement is seen for radial position larger than about 0.85 nm, which is in the multilayer region, where the adsorbed density is large (cf. inset of Fig. 2). Some error is seen in the inner region, $0 \leq r \leq 0.85$ nm, but is not of consequence since the density here is much lower, and the contribution to the pore flux is therefore negligible. The cause of the deviation is most likely due to the inadequacy of a viscous model in this low-density region where the mean-free path is large, and is being further explored despite its insignificance.

The abrupt increase of the wall friction coefficient to very large values leading to the no-slip condition at a critical density is clearly due to the well-known failure of the kinetic theory at high density. Comparison of the estimated mean-free path of about 0.22 nm at density of 10 nm^{-3} and 0.027 nm at density of 80 nm^{-3} with the depth of penetration beyond the potential minimum of about 0.05 nm (cf. inset of Fig. 2), indicates that interactions between molecules in this region will be important at sufficiently high density. Consequently, diffuse wall reflection will dissipate the collective axial momentum in this region, leading to the no-slip condition which is clearly evident in Fig. 3.

It is now clear from the above results that a combination of momentum transfer at the wall and viscous transport in the fluid suffices to explain the transport behavior of pure component fluids in nanopores. The mechanism of Knudsen diffusion commonly assumed to occur in mesopores and micropores is not manifested because of the well-known [21] localization of adsorbed molecules near the pore wall at the position of the potential minimum. In the past, such adsorptive localization has been regarded [11,12,21] as giving rise to a surface flow phenomenon that may be recognized as arising from the momentum transfer mechanism demonstrated here. Further, while we have performed calculations here for a mesopore of about 4 nm diameter, in smaller pores, although viscous momentum transfer will still operate, the effect of slip due to momentum loss at the wall may be even more important because of the stronger dispersive forces and greater degree of localization at the pore wall (except for a narrow range of pore size where the overlap of potential can lead to a broad minimum). While this is the case for real porous materials with adsorbing surfaces, in hard sphere systems the localization is absent and Knudsen flow may indeed occur.

A further attractive feature of our proposal is that it contains the necessary ingredients to model the "activated diffusion" process attributed to micropores where the contribution of viscous flow is very small [3,4,11]. Except for high densities if we approximate $\rho(r) \sim \exp[-\Phi(r)/k_BT]$, where $\Phi(r)$ is the position-dependent fluid-solid potential, it is readily seen that the first term on the right-hand side of Eq. (7) will predict a diffusivity $D_o \propto e^{a\Phi_m/k_BT}$, where a is positive constant smaller than unity and $\Phi_m = \Phi(r_0)$ (the minimum value). The effective activation energy $E_D = a|\Phi_m|$ is in line with that empirically postulated and widely used in the literature in interpreting adsorption kinetics in carbons and a variety of other adsorbents [3,4,11]. However, besides such adsorbents the same mechanisms will apply to membranes, biological systems, and a variety of other systems involving transport in ultrafine pores.

This research has been supported by a grant from the Australian Research Council under the Large Grants Scheme. The authors are also grateful to Dr. Owen Jepps for useful discussions.

*Author to whom correspondence may be addressed.
†Permanent address: Computational and Structural Group, Department of Chemistry, Imperial College, London SW72AY, England.

[1] M. E. Davis, Nature (London) **417**, 813 (2002).
[2] S. Ijima, Nature (London) **354**, 56 (1991).
[3] S. K. Bhatia, Proc. R. Soc. London A **446**, 15 (1994).
[4] S. K. Bhatia, in *Advances in Transport Processes IX*, edited by A. S. Mujumdar and R. A. Mashelkar (Elsevier, Amsterdam, 1993).
[5] D. Nicholson and K. Travis, in *Recent Advances in Gas Separation by Microporous Membranes*, edited by N. Kanellopoulos (Elsevier, Amsterdam, 2000).
[6] E. A. Mason, A. P. Malinauskas, and R. B. Evans, J. Chem. Phys. **46**, 3199 (1967).
[7] R. Jackson, *Transport in Porous Catalysts* (Elsevier, Amsterdam, 1977).
[8] M. P. Allen and D. J. Tildesley, *Computer Simulation of Liquids* (Clarendon, Oxford, 1987).
[9] R. F. Cracknell, D. Nicholson, and N. Quirke, Phys. Rev. Lett. **74**, 2463 (1995).
[10] J. H. Petropoulos and G. K. Papadopoulos, J. Membr. Sci. **101**, 127 (1995).
[11] J. Kärger and D. M. Ruthven, *Diffusion in Zeolites and Other Microporous Solids* (Wiley, New York, 1992).
[12] R. M. Barrer, in *The Gas Solid Interface*, edited by E. A. Flood (Marcel Dekker, New York, 1967), Vol. 2.
[13] D. Nicholson, J. Membr. Sci. **129**, 209 (1997).
[14] K. D. Travis and K. E. Gubbins, Mol. Simul. **25**, 209 (2000).
[15] G. Arya, H.-C. Chang, and E. Maginn, J. Chem. Phys. **115**, 8112 (2001).
[16] M. Kruk and M. Jaroniec, Chem. Mater. **12**, 222 (2000).
[17] D. J. Evans and G. P. Morriss, *Statistical Mechanics of Nonequilibrium Liquids* (Academic, London, 1990).
[18] T. H. Chung, M. Ajlan, L. L. Lee, and K. E. Starling, Ind. Eng. Chem. Res. **27**, 671 (1988).
[19] I. Bitsanis, T. K. Vanderlick, M. Tirrell, and H. T. Davis, J. Chem. Phys. **89**, 3152 (1988).
[20] P. G. de Gennes, Langmuir **18**, 3413 (2002).
[21] D. Nicholson and J. H. Petropoulos, Ber. Bunsen-Ges. Phys. Chem. **79**, 796 (1975).